

PACS 42.55.Lt; 42.60.Lh
DOI: 10.1070/QE2001v031n03ABEH001919

Kinetic model of the active medium of a He–Ar laser pumped by a hard ioniser

D N Babichev, A V Karelin, O V Simakova, H Tomizawa

***Abstract*. A detailed nonstationary model of a He – Ar laser pumped by a hard ioniser is developed. It is found by numerical simulation that the pumping of the upper laser level is governed either by the three-body recombination of atomic argon ions with electrons or the dissociative recombination of molecular argon ions with electrons, depending on the argon content in a gas mixture. The conversion of dimer molecular argon ions into trimers, the quenching of the upper laser level by neutral atoms, and the spectral line broadening determine the optimum lasing conditions for the total mixture pressure and the partial argon pressure for different excitation conditions. The model adequately describes experiments using electron beam and nuclear pumping. The optimisation of a 1.79-μm nuclear-pumped He – Ar laser in the VIR-2M reactor gave a maximum laser efficiency of 1.2 %.**

Keywords: *nuclear-pumped lasers, plasma lasers, electron-beam pumping, kinetics, plasma chemistry*.

1. Introduction

High-pressure lasers operating on atomic transitions of inert gases remain for a long time one of the most promising systems for producing high-power lasing in the near IR region. Their main advantages are low pump thresholds, a long service life, the nontoxicity of the active medium, and the feasibility of lasing on several wavelengths. The Xe laser was most extensively studied using different pump methods, pump powers, and compositions of the active medium, because it has the lowest excitation threshold and the highest efficiency [1 – 6]. In particular, the kinetics of processes in its active medium was studied in many papers [7 – 17].

Lasers on atomic transitions of other inert gases, including argon, were studied less comprehensively. Lasing on argon atoms was obtained on the transitions between 3d and 4p levels, using He – Ar and He – Ne – Ar mixtures pumped by electron and ion beams [18-25], the electric discharge [20], and fission fragments of nuclear reactions [3 – 5, 7, 26 – 32]. Lasing at $\lambda = 1.27$ and 1.79 μm was studied in greatest detail. For these wavelengths, the maximum laser parameters were obtained: laser efficiency above 1 % [27 – 29], radiation power up to 1 kW in a nuclear-pumped laser [7], and an output energy of 2 J in an electron-beam-pumped laser [18, 21]. These data are considerably worse than the characteristics of the Xe laser. However, a similar structure of terms of argon and xenon atoms, the similarity of kinetic processes in mixtures of inert gases, and the fact that the upper laser level of the transition at $\lambda = 1.79$ μm in the Ar laser is the lowest one in its multiplet offer promise for a substantial improvement of the present-day output parameters of the Ar laser. It seems reasonable to construct the kinetic model of its active medium and use it for estimating potentialities of this laser.

Many problems of kinetics of the Ar laser, including the mechanism of inversion, are yet unsolved despite efforts to construct a laser model in Refs [33 – 35]. These papers differ in the mechanisms proposed for pumping the upper laser level. The pumping was thought to be governed by the dissociative recombination (DR) of molecular Ar^{2+} ions with electrons [33], the dissociative recombination of heteronuclear $HeAr^+$ ions with electrons [34], and the three-body recombination (TBR) of atomic Ar^+ ions with electrons [35].

A common disadvantage of these models is that they are related to one experimental setup (which, as a rule, makes them inapplicable for other conditions) and that each of them uses a high (up to 100 % [34, 35]) selectivity of direct population of the upper laser level, which contradicts to the spectroscopic studies of plasma relaxation in mixtures of inert gases [36]. As for the model [34], which uses the dissociative recombination of $HeAr^+$ ions as the pump reaction, it ignores the key process involving these ions, namely, their disintegration by He atoms that is accompanied by the production of Ar^+ (this is an inverse reaction with respect to the formation of $HeAr^+$ from Ar^+ in the reaction of three-body conversion involving two He atoms). Because of a very low binding energy (26.7 meV [36]), this reaction should proceed rapidly and should strongly affect on the equilibrium concentration of both ions. According to our estimates, its rate (in $cm^3\ s^{-1}$) is $1.7 \times 10^{-10} e^{-26.7 meV/T_g}$, where T_g is the gas temperature. Using the model proposed in Ref. [34], we made the test calculation for two cases (taking into account the disintegration of $HeAr^+$ ions and ignoring this reaction), which showed that the absence of the disintegration reaction under optimum lasing conditions leads to the overstatement of the pump flux to the upper laser levels during the dissociative recombination of $HeAr^+$ ions by a factor of ten. Because of this error, which is of principal importance, and some other errors in the description of kinetics of a He – Ar plasma, the conclusions and the results of Ref. [34] are inapplicable for the understanding of operation of the He – Ar laser.

D N Babichev, A V Karelin, O V Simakov General Physics Institute, Russian Academy of Sciences, ul. Vavilova 38, 119991 Moscow, Russia
H Tomizawa Japan Synchrotron Radiation Research Institute, 1-1-1 Kouto, Mikazuki-cho, Sayo-Gun, Hyogo 679-5198, Japan

Received 29 September 2000
Kvantovaya Elektronika **31** (3) 209 – 217 (2001)
Translated by A N Kirkin

The aim of this paper is to construct a detailed nonstationary kinetic model of the active medium of the argon laser that takes into account a possible presence of impurity molecular gases N_2, O_2, H_2, and H_2O and is suitable for the description of various experiments using different excitation methods. In the calculations, we used the modified PLASER code [37].

2. Kinetics of plasma-chemical processes in a He–Ar mixture

In the kinetic model of a He – Ar laser operating on a mixture with impurities of molecular gases N_2, O_2, H_2, and H_2O, we took into account 46 plasma components: atomic and molecular argon and helium ions He^+, He_2^+, He_3^+, Ar^+, Ar_2^+, Ar_3^+, $HeAr^+$, metastable states of a helium atom He^*, helium and argon dimers He_2^* and Ar_2^*, and atomic and molecular ions of impurity gases N^+, O^+, H^+, N_2^+, O_2^+, H_2^+, and H_2O^+. We took into account all the excited levels of atomic argon belonging to the states $3d$, $3d'$, $4p$, $4p'$, $4s$, and $4s'$. The diagram of these levels and the main transitions in the argon atom are presented in Fig. 1a. The kinetics of levels of the argon atom includes radiative transitions between the levels of the above-mentioned configurations, the quenching of excited levels by He and Ar atoms, and all possible electron mixing reactions for allowed transitions. The rate constants for electron mixing for allowed transitions were calculated by the formula of Van Regemorter [38], using oscillator strengths and decay probabilities from Ref. [39]. For the transition at 1.79 μm, the decay probability was taken equal to 1.1×10^6 s^{-1} [40]. For emission on the transitions from the resonance levels $^1s_2$ ($^1P_1$) and $^1s_4$ ($^3P_1$) to the ground argon state $^1S_0$, we took into account the effect of reabsorption. For these transitions, the decay probabilities were multiplied by the escape factor θ calculated in the plane geometry [41].

The experimental data on the rate constants of quenching of the excited states $3d$ and $3d'$ by helium and argon atoms are absent in the literature. In the models [33, 34], values of 2×10^{-12} cm^3 s^{-1} [33] for helium and 6×10^{-10} [33] and 10^{-11} cm^3 s^{-1} [34] for argon were used for the $3d[3/2]_{0,1}$ level, which represents the upper laser level for the transition at 1.79 μm. For helium and argon, we used the values 3×10^{-12} and 3×10^{-11} cm^3 s^{-1}, respectively, which were obtained from the best fit of experiments. The quenching rate constants that were used for other levels of the $3d$, $3d'$ configuration, which are characterised by very narrow energy spacings in multiplets and between them (of the order of 0.01 eV), were higher by an order of magnitude, 5×10^{-11} cm^3 s^{-1}. The rate constants of direct and inverse processes were interrelated by the principle of detailed balancing.

The cross sections for stimulated emission on the $i - j$ transitions with the wavelength λ_{ij} and the probability A_{ij} of the radiative decay of the upper laser level were calculated by the formula

$$\sigma_{ij}^{\mathrm{st}} = \frac{A_{ij}\lambda_{ij}^2}{4\gamma},$$

where $\gamma = \gamma_\mathrm{d} + \pi^2 \Delta\nu_{\mathrm{col}}$ is the effective linewidth;

$$\gamma_\mathrm{d} = \gamma_0 \frac{(2T_\mathrm{g})^{1/2}}{c\mu};$$

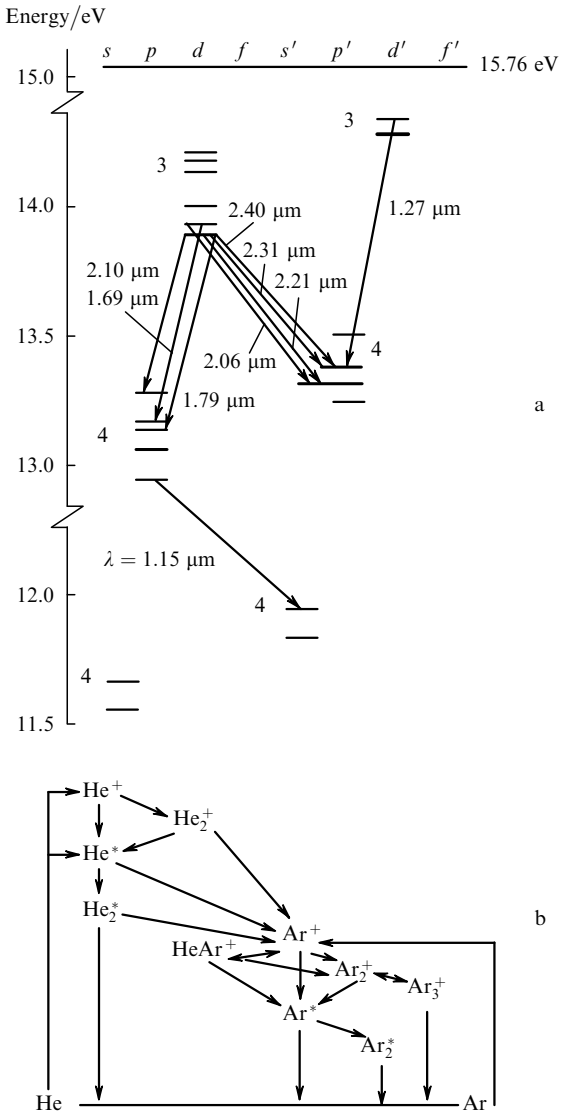

Рис.1. Energy level diagram of the Ar atom (a) and the scheme of plasma-chemical reactions in the He – Ar mixture (b).

γ_0 is the cyclic frequency of emission; μ is the mass of an Ar atom; $\Delta\nu_{\mathrm{col}}$ is the collisional linewidth; and c is the speed of light.

Experimental data on collisional line broadening for the transitions under consideration are unavailable. For the 1.79-μm line, we used $\Delta\nu_{\mathrm{col}} = 5.94 \times 10^9$ s^{-1} bar^{-1} for broadening by helium and $\Delta\nu_{\mathrm{col}} = 7.2 \times 10^{10}$ s^{-1} bar^{-1} for broadening by argon. These values were obtained from the best fit of calculation results to experimental data.

The ionising capacity of a pump source, which is characterised by the pump power density (specific input power) P_p, was determined by the ionisation frequency ν_i, which was calculated by the formula

$$\nu_\mathrm{i} = P_\mathrm{p}(1.3E_\mathrm{p}N)^{-1},$$

where E_p is the energy of electron–ion pair formation, which is equal to 42 and 26 eV for helium and argon, respectively; and N is the gas concentration. The coefficient 1.3 in the formula takes into account the pump power loss through

excitation of inert gas atoms by electrons from the ground state.

In the case of pumping by an electron beam with the current density j and the electron energy E, the pump power density was calculated by the formula

$$P_p = 1.3\,\frac{\Delta E}{\Delta x}\,\frac{p_{mx} j}{e},$$

where $\Delta E/\Delta x$ is the energy lost by electrons of the beam on a path 1 cm long in a mixture at a pressure $p_{mx} = 1$ bar. For the electron energy $E = 300$ keV, the values of $\Delta E/\Delta x$ were taken from Ref. [6], where the free electron path x_{run} in argon was experimentally determined. According to Ref. [42], the ratio $\Delta E/\Delta x$ for three inert gases He, Ar, and Xe in [6] was calculated by the formulas

$$\frac{\Delta E}{\Delta x} = \frac{E}{0.4 x_{run}},$$

$$x_{run} = \frac{R_0}{\rho}\,\frac{A}{Z}\,\frac{E^2}{mc^2(mc^2+E)},$$

where $R_0 = 0.27$ g cm^{-2}; ρ is the gas density; A and Z are the atomic weight of an element and its number; and m is the electron mass. Using the same formulas, we calculated $\Delta E/\Delta x$ for other electron energies.

In the case of nuclear pumping with ^{235}U fission fragments, which escape from uranium layers of volume V_f into a laser cell of volume V_g under its irradiation by thermal neutrons with the flux density F, the pump power density P_p is determined by the expression [43]

$$P_p = \varepsilon E_f F \sigma_f N_5 V_g V_f^{-1},$$

where ε is efficiency of energy transfer from fission fragments to a gas [44]; E_f is the fission fragment energy; σ_f is the cross section for ^{235}U fission by thermal neutrons; and N_5 is the concentration of ^{235}U nuclei.

In a He – Ar mixture pumped by a hard ioniser, ions and excited states of helium and argon are formed (Fig. 1b presents the diagram of plasma-chemical reactions, and Table 1 presents the basic reactions in the He – Ar mixture). Then, molecular ions He_2^+, Ar_2^+, and $HeAr^+$ are produced in three-body conversion reactions (1) – (5). The $HeAr^+$ ions are disintegrated by helium atoms in reaction (6), with the rate constant related to the rate constant of reaction (5) via the equilibrium constant $K_{eq} = 1.7 \times 10^{22}(26\,\text{meV}/T_g)^{-3/2} \times e^{-26.7\text{meV}/T_g}$, and participate in reconstruction reaction (7), which produces molecular Ar_2^+ ions, or dissociatively recombine producing Ar^*.

In reactions of three-body conversion of Ar_2^+ molecular ions (8) and (9), Ar_3^+ molecular ions are produced, which are either destroyed in reverse reactions, with rate constants related to the rate constants of reactions (8) and (9) via the equilibrium constant $K_{eq} = 3.86 \times 10^{21}(26\,\text{meV}/T_g)^{-3/2} \times e^{-0.22\,\text{eV}/T_g}$ or dissociatively recombine in reaction (10), producing argon atoms in the ground state. The relationship between the fluxes of these processes and the dissociative recombination of Ar_2^+, which depends on the pump power density and the argon pressure, determines the optimum concentration of Ar_2^+ ions.

In the case of a strongly diluted He – Ar mixture [$\delta_{Ar} = [Ar]/([He] + [Ar]) = 0.0001 - 0.1$], the major portion of the pump energy is deposited into helium, and the energy is transferred from helium to argon ions in Penning and charge exchange reactions (11) – (13). Because the cross section for argon ionisation by electrons exceeds the cross section for

Табл.1. Basic reactions in a He–Ar mixture and their rate constants.

Reaction number	Reaction	Rate constant/ cm$^{3(n-1)}$ s^{-1}	References
(1)	$He^+ + 2He \rightarrow He_2^+ + He$	$2.6\cdot10^{-33}/T_g$	[45]
(2)	$He^+ + He + Ar \rightarrow He_2^+ + Ar$	$0.8\cdot10^{-33}/T_g$	[46]
(3)	$Ar^+ + 2Ar \rightarrow Ar_2^+ + Ar$	$2.5\cdot10^{-31}(0.026/T_g)^{0.75}$	[47]
(4)	$Ar^+ + Ar + He \rightarrow Ar_2^+ + He$	$1.5\cdot10^{-31}(0.026/T_g)^{0.75}$	[53]
(5)	$Ar^+ + He + He \rightarrow HeAr^+ + He$	$10^{-32}(0.026/T_g)^{0.75}$	estimate
(6)	$HeAr^+ + He \rightarrow Ar^+ + 2He$	$1.7\cdot10^{-10}(0.026/T_g)^{-0.75}e^{-0.0267/T_g}$	$K_5 k_{eq}$
(7)	$HeAr^+ + Ar \rightarrow Ar_2^+ + He$	$3.6\cdot10^{-9}$	[49]
(8)	$Ar_2^+ + Ar + Ar \leftrightarrow Ar_3^+ + Ar$	$1.2\cdot10^{-31}(0.026/T_g)^{0.75}$	estimate
(9)	$Ar_2^+ + Ar + He \leftrightarrow Ar_3^+ + He$	$3.5\cdot10^{-32}(0.026/T_g)^{0.75}$	estimate
(10)	$Ar_3^+ + e \rightarrow 3Ar$	$10^{-6}(0.026/T_e)^{0.5}$	[50]
(11)	$He^* + Ar \rightarrow Ar^+ + e + He$	$1.3\cdot10^{-10}(T_g/0.026)$	[48]
(12)	$He_2^+ + Ar \rightarrow Ar^+ + 2He$	$2\cdot10^{-10}$	[49]
(13)	$He_2^+ + Ar + He \rightarrow Ar^+ + 3He$	$5\cdot10^{-31}$	estimate
(14)	$He^* + He + Ar \rightarrow He_2^* + Ar$	$1.85\cdot10^{-33}e^{-0.067/T_g}$	[46]
(15)	$He^* + 2He \rightarrow He_2^* + He$	$2\cdot10^{-33}e^{-0.067/T_g}$	[45]
(16)	$Ar^* + 2Ar \rightarrow Ar_2^* + Ar$	$3.3\cdot10^{-32}(0.026/T_g)^{0.75}$	[47]
(17)	$Ar^* + Ar + He \rightarrow Ar_2^* + He$	$10^{-32}(0.026/T_g)^{0.75}$	estimate
(18)	$Ar^* + He + He \rightarrow HeAr^* + He$	$5\cdot10^{-35}(0.026/T_g)^{0.75}$	estimate
(19)	$Ar_2^+ + e \rightarrow Ar^* + Ar$	$7.37\cdot10^{-8}T_e^{-0.67}$	[36]
(20)	$Ar^+ + e + e \rightarrow Ar^* + e$	$5.4\cdot10^{-27}/T_e^{-4.5}$	[51]
(21)	$Ar^+ + e + (He, Ar) \rightarrow Ar^* + (He, Ar)$	$2.4\cdot10^{-31}T_g T_e^{-3.5}$	[51]
(22)	$Ar^* + Ar^* \rightarrow Ar^+ + e + Ar$	$1.2\cdot10^{-9}$	[52]

Notes: n is the number of reagents; the gas temperature T_g and electron temperature T_e are measured in electronvolts.

helium ionisation by a factor of more than ten [54], the role of channels of direct ionisation and excitation of argon by electron impact increases against the background of reactions (11)–(13) even for $\delta_{Ar} \geqslant 0.01$. Excited He^* and Ar^* atoms form excimer molecules He_2^*, Ar_2^*, and $HeAr^*$ in reactions (14)–(18), which rapidly radiatively decay to the ground state.

Under a great variety of pumping conditions, argon atoms in the He–Ar mixture are accumulated in great amounts (at the concentration of the order of 10^{15} cm^{-3}) in metastable and resonance $4s$ states because of low probabilities ($\sim 10^{15}$ s^{-1}) of their loss in association reactions (16)–(18) and through electron quenching to the ground state [the rate constants of reactions (17), (18) were assumed to be of the order of the corresponding constants for the xenon atom [55]). The strongest channel of loss of the Ar ($4s$) states is chemiionisation (22), which has a high rate constant (see Table 1). In this reaction, atomic argon ions are formed, which are subsequently again involved in recombination. This process determines energy recirculation in the He–Ar laser and, as calculations show, is capable of providing as large as 50 % of the total efficiency. The effect of chemiionisation on the He–Ar laser efficiency has been first reported in Ref. [25]. As shown in [16], a similar situation occurs in the He–Xe laser.

A He–Ar laser mixture was found to be sensitive to the presence of impurities. The He^+, He_2^+, He^*, Ar^+, Ar_2^+, and Ar^* components of the plasma of working gases easily transfer the pump energy to atomic and molecular components of impurities in charge exchange, Penning, and excitation transfer reactions (a detailed kinetics in (He, Ar) $- N_2 - O_2 - H_2 - H_2O$ mixtures is presented in [56, 57]).

The total number of plasma-chemical reactions considered in the model, including the level kinetics and the processes involving molecular gases, is as large as 500. We calculated the concentrations of plasma components taken into account in the model, electron and gas temperatures, the laser efficiency, the power and energy of output radiation, and the unsaturated gain coefficient.

2.1. Mechanisms of inversion production at the laser transitions

In the kinetic model, we considered laser transitions at the wavelengths 1.27 μm ($3d'[3/2]_1 - 4p'[1/2]_1$), 1.79 μm ($3d[1/2]^o_{0,1} - 4p[3/2]_{2,1}$), and 2.40 μm ($3d[1/2]^o_0 - 4p'[1/2]_1$). Particular attention was given to the transition at 1.79 μm, and this line was used for optimising the model. The 1.79-μm line belongs to two pairs of closely spaced ($\Delta E \sim 18$ meV) levels and, therefore, this transition was treated as one transition with combined pairs of upper and lower levels. To determine the pumping mechanism for the upper laser level, we carried out a detailed analysis of the behaviour of plasma component concentrations and fluxes of different reactions as functions of mixture pressure p_{mx}, argon pressure p_{Ar}, and pump power.

We found that three processes can be involved in the pumping of the upper laser level: three-body recombination of Ar^+ ions, dissociative recombination of $HeAr^+$ ions, and dissociative recombination of Ar_2^+ ions. The role of each of the processes depends on the argon content δ_{Ar} in a mixture. For $\delta_{Ar} \leqslant 10^{-3}$, the major argon components in a mixture are atomic Ar^+ ions. The flux of three-body recombination of Ar^+ with electrons transferes the main pump flux. In this case, the fluxes of DR of $HeAr^+$ and Ar_2^+ ions are equal to 15 % – 25 % and 5 % – 20 %, respectively, of the total pump flux depending on p_{mx}. The fraction of DR of $HeAr^+$ ions increases with increasing p_{mx} because the fluxes of $HeAr^+$ formation in reaction (5) and its disintegration in reverse reaction (6) are quadratic and linear functions of p_{mx}, respectively.

A further increase in δ_{Ar} causes an increase in the electron temperature, and conversion (4) and charge exchange (7) reactions cause a decrease in the concentration of atomic Ar^+ ions and molecular $HeAr^+$ ions and an increase in the concentration of molecular Ar_2^+ ions. Because of this, the role of fluxes of TBR of Ar^+ ions and DR of $HeAr^+$ decreases, whereas that of the flux of DR of Ar_2^+ increases. When $\delta_{Ar} \geqslant 0.01$, the dominant relaxation flux corresponds to dissociative recombination. This suggests conclusions concerning the basic pumping mechanism for the upper laser level of the argon atom.

A specific feature of the transition at 1.79 μm is that the upper laser level $3d[1/2]^o_{1,0}$ is the lower level in its configuration. Because of this, a large fraction of the relaxation flux can be transferred via this level. One may attribute to this fact preferential lasing on this wavelength in a high-pressure laser, such as the He–Ar laser, even without the assumption that the direct population of this level is purely selective.

Experimental data on the channels of three-body recombination of atomic ions are unavailable. It is reasonable to assume that first, due to three-body recombination, highly excited states (above $3d$ and $3d'$) of the argon atom are populated and then, in the course of the radiative-collisional cascade from these levels the states $3d$ and $3d'$ are populated. For the best description of experimental results, we needed 35 % and 12 % of the TBR flux, which were directed to the levels $3d[1/2]^o_{1,0}$ ($\lambda = 1.79$ μm and 2.4 μm) and $3d'[3/2]_1$ ($\lambda = 1.27$ μm), respectively either directly or through radiative transitions from high-lying levels that were not taken into account in the model. The remaining portion of the TBR flux was distributed over the states $4p$, $4p'$, $3d$, and $3d'$.

Because of a small depth of the $HeAr^+$ potential well (26.7 meV), it is natural to assume that during dissociative recombination of these ions the highly excited states of the argon atom are populated. In the model, all the levels $3d$ and $3d'$ were assumed to be identically populated due to dissociative recombination of $HeAr^+$. We determined the partial fraction of the DR flux directed to the upper laser level using the results of Ref. [36]. It was found in [36] in the study of relaxation of collisionless plasma of inert gases that the dominant portion (above 90 %) of the DR flux of the molecular Ar_2^+ ion was transferred in the lines starting from the $4p$ and $4p'$ levels of the argon atom. However, on the basis of these results, one can make conclusions concerning the fluxes to the $3d$ and $3d'$ levels under the assumption that thee $4p$ and $4p'$ levels are populated through radiative transitions from the $3d$ and $3d'$ levels of the argon atom.

We distributed the partial DR flux reported in Ref. [36] in accordance with the probabilities of decay for these transitions and found that approximately 15 % of the pump flux directly reached the $3d[1/2]^o_{1,0}$ level (the upper level for the 1.79-μm line) and that approximately 12 % of the pump flux reached the $3d'[3/2]_1$ level (the upper level for the 1.27-μm line). Approximately 25 % of the pump flux, both in TBR and DR, directly reached the $4p$ and $4p'$ levels. Thus, one can see that the portion of the relaxation flux going in the radiative-collisional cascade via the lower laser level is greater that the portion going via the upper level. Because of this, the quen-

ching of the active laser levels is of substantial importance for obtaining population inversion.

According to the calculations by the Van Regemorter formula [38], using the decay probabilities from Ref. [39], the total rate constants for electronic mixing of the upper and lower laser levels for the 1.79-μm line are equal to $1.8\times 10^{-7}/T_e^{0.5}$ and $1.1\times 10^{-7}/T_e^{0.5}$ cm^3 s^{-1}, respectively, where T_e is the electron temperature in eV. Therefore, the population inversion for the laser transitions under actual operating conditions is predominantly determined by the quenching by buffer gas atoms. As mentioned above, the rate constants of these processes were chosen in the course of simulation because the corresponding experimental data are unavailable in the literature. The $4p'[1/2]_0$ state is 0.374 eV below the upper laser level $3d[1/2]^o_{1,0}$, and this energy gap is much greater than the corresponding energy gap for the lower laser level (0.076 eV). Because of this it is reasonable to assume that the probability of quenching the lower laser level by helium atoms is higher than the quenching probability for the upper laser level. To obtain the best fit with the experimental results, the rate constant for quenching the lower laser level by helium was taken equal to 7×10^{-12} cm^3 s^{-1}.

3. Numerical simulation of the He–Ar laser

3.1. Model testing

The kinetic model was tested using the results of experiments with electron-beam-pumped [20, 23] and nuclear-pumped [4, 5, 27] lasers. In Refs [20, 23], experiments were carried out on the 'Tandem' laser system. The laser was pumped by an electron beam with electron energy of 300–320 keV. For pulses ~ 2 μs [20] and 5 μs [23] long at the base, the electron current density reached 1.8 A cm^{-2} [20] and 1.7 A cm^{-2} [23]. In particular, a He–Ar mixture was studied in both works [20, 23], and the authors optimised for it the energy characteristics by varying p_{mx} from 0.5 to 3.5 bar and the relative argon content δ_{Ar} from 10^{-4} to 0.1. The laser energy Q_g and the laser efficiency η, which was calculated as the ratio to the energy deposited in the active medium, are presented there as the output energy characteristics. Because the input energy in Refs [20, 23] differs from the value calculated by us using the results reported by these authors in the recent paper [6] by a factor of about two, we tested the model for the results of experiments [20, 23] using the output laser energy as the basic parameter.

In Ref. [23], the He : Ar = 100 : 1 mixture gave the optimum efficiency throughout the entire range of p_{mx} studied there. The maximum output energy $Q_g = 1.73$ J was reached for the maximum $p_{mx} = 3.5$ bar. Similar results were obtained in the calculation. Fig. 2 presents the experimental [23] and the calculated dependences of Q_g on δ_{Ar} for the total $p_{mx} = 3.5$ bar. In the calculation, the maximum $Q_g = 2.5$ J with $\eta = 0.8\,\%$ was also obtained for $p_{mx} = 3.5$ bar and $\delta_{Ar} = 10^{-2}$.

In Ref. [20], similar optimum operating laser conditions were obtained. Fig. 3a presents the experimental [20] and calculated dependences of the total radiation energy Q_g on p_{mx} for different δ_{Ar}. For convenience of the analysis, the same results are presented in Fig. 3b in the form of the dependence of Q_g on δ_{Ar} for different p_{mx}. One can see (Fig. 3a) that when $\delta_{Ar} < 5\times 10^{-2}$, Q_g increases with increasing p_{mx}. This dependence is violated with increasing δ_{Ar}. For $\delta_{Ar} = 5\times 10^{-2}$ and 0.1, the output laser energy begins to

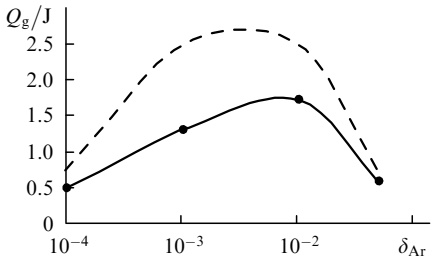

Рис.2. Experimental (solid curve, [23]) and calculated (dashed curve) dependences of the total output laser energy Q_g on the argon content δ_{Ar} in the He–Ar mixture for $p_{mx} = 3.5$ bar, $j = 1.7$ A cm^{-2}, $E \sim 320$ keV, pump pulse duration $\tau_p \sim 5$ μs, and the calculated electron temperature $T_e \simeq 0.18 - 0.37$ eV.

decrease with increasing pressure at $p_{mx} = 2.5$ and 1.5 bar in the experiment and at 2 and 1 bar in the calculation, respectively. One can see from Fig. 3b that the optimum δ_{Ar}, like in Ref. [23], is 10^{-2} for all p_{mx} under study. Both an increase and a decrease in δ_{Ar} caused a decrease in the output laser energy. The maximum $Q_g = 0.76$ J in the experiment [20] and 1.1 J in the calculation were obtained for $p_{mx} = 3.5$ bar and $\delta_{Ar} = 10^{-2}$. In the experiment [20], the maximum efficiency was obtained for $p_{mx} = 2.5$ bar and the same δ_{Ar}. The maximum calculated efficiency $\eta = 0.97\,\%$ was obtained

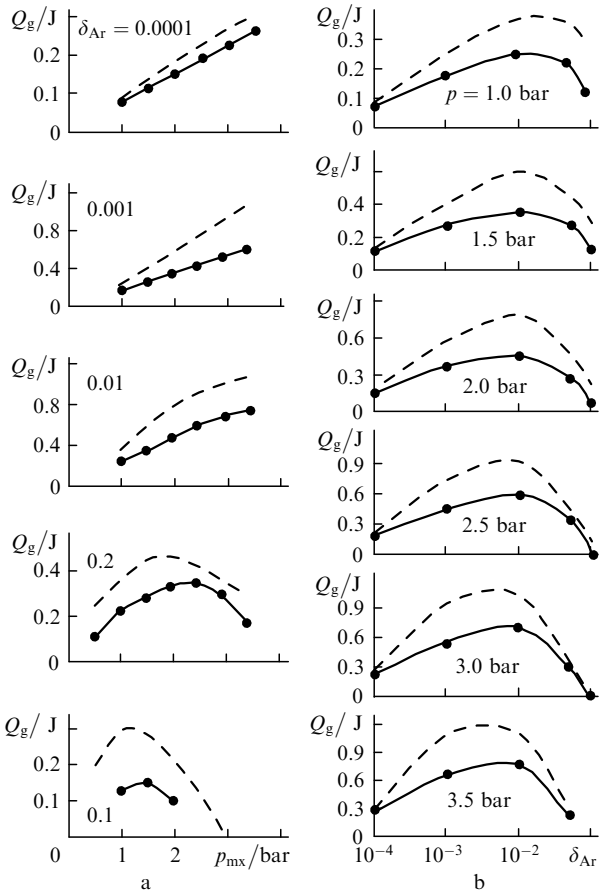

Рис.3. Experimental (solid curves, [20]) and calculated (dashed curves) dependences of the total output energy Qg of the He–Ar laser on the mixture pressure p_{mx} for different argon contents δ_{Ar} (a) and on δ_{Ar} for different p_{mx} (b) for $j = 1.8$ A cm^{-2}, $E \sim 300$ keV, $\tau_p \sim 2$ μs, and $T_e = 0.18 - 0.42$ eV.

for $p_{mx} = 1.5$ bar. The calculation of Q_g as a function of p_{mx} for the experimental conditions [20, 23] in the region of high pressures showed that maximum energies of 1.15 J [20] and 2.6 J [23] were achieved for $p_{mx} = 4.5-5.5$ atm. In the case of a cavity with a higher Q-factor, maximum energies of 1.55 J [20] and 3.5 J [23] were achieved for $p_{mx} = 9-10$ bar.

In Fig. 4, we compare the calculated and the experimental [5] dependences of the laser efficiency η at $\lambda = 1.79$ μm on p_{Ar} for He–Ar mixtures with total pressures of 1, 2, and 3 bar and high-power nuclear pumping (~ 1 kW cm^{-3}) by the pulsed EBR-L reactor [58, 59]. For p_{mx} varied in the range from 1 to 3 bar, the input energy density per pulse for pulses 0.4 ms long at the base varied from 0.065 to 0.15 J cm^{-3} (the peak specific input power varied from 360 to 840 W cm^{-3}) [59]. In the experiment, $p_{mx} = 1$ bar and $p_{Ar} \approx 2$ Torr ($\delta_{Ar} \approx 2.5 \times 10^{-3}$) were the optimum parameters for obtaining the maximum laser efficiency (1.05 %). For $p_{mx} = 2$ and 3 bar, maximum efficiencies of 1 and 0.88 %, respectively, were reached for higher p_{Ar} (3 and 2.5 Torr), but for approximately the same δ_{Ar} (2×10^{-3} and 10^{-3}). In the calculations, the maximum efficiency $\eta = 1.16$ % was obtained for $p_{mx} = 1$ bar and a partial argon pressure of 5 Torr ($\delta_{Ar} \approx 6.5 \times 10^{-3}$). The maximum laser efficiencies for $p_{mx} = 2$ and 3 bar were 1.11 and 0.97 %, respectively, and they were achieved at lower p_{Ar} (4 and 3 Torr; $\delta_{Ar} \approx 2.5 \times 10^{-3}$ and 1.3×10^{-3}). In our opinion, the spread of the optimum p_{Ar} in the experimental dependence on p_{mx} is associated with a small number of experimental points. The analysis of the experimental curve for $p_{mx} = 1$ bar showed that the optimum p_{Ar} was found in a range of 2–8 Torr.

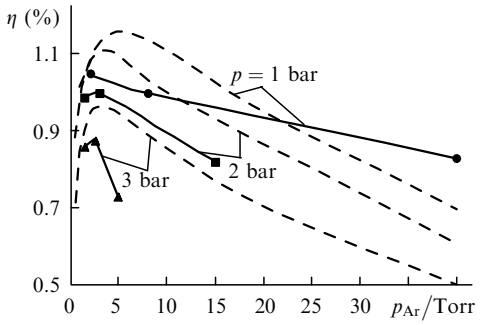

Рис.4. Experimental (solid curves, [5]) and calculated (dashed curves) dependences of the laser efficiency at $\lambda = 1.79$ μm on the Ar pressure for different pressures of the He–Ar mixture and $T_e \simeq 0.12 - 0.26$ eV.

The comparison of the calculation results with the experimental data of Ref. [27], which were obtained on the SPR-III reactor, is presented in Fig. 5. It shows the threshold specific input power and the ratio of the instantaneous efficiency η' at the moment when the specific input power is equal to 75 W cm^{-3} to the laser efficiency at $p_{mx} = 1$ bar as functions of p_{mx} for $\lambda = 1.79$ μm. The specific input power at the peak of the pump pulse for a helium pressure of 1 bar was 240 W cm^{-3}; the length of the pump pulse at the base was about 2.5 ms, and $\delta_{Ar} = 3 \times 10^{-3}$.

The maximum laser efficiency was 1.4 ± 0.4 % in the experiment and 1.18 % in the calculation (Fig. 5a), and it was reached at $p_{mx} = 750$ Torr. The minimum threshold input power densities in the experiment (3 W cm^{-3}) and in the calculation (0.85 W cm^{-3}) correspond to $p_{mx} = 250$ Torr and increase with increasing p_{mx} (Fig. 5b).

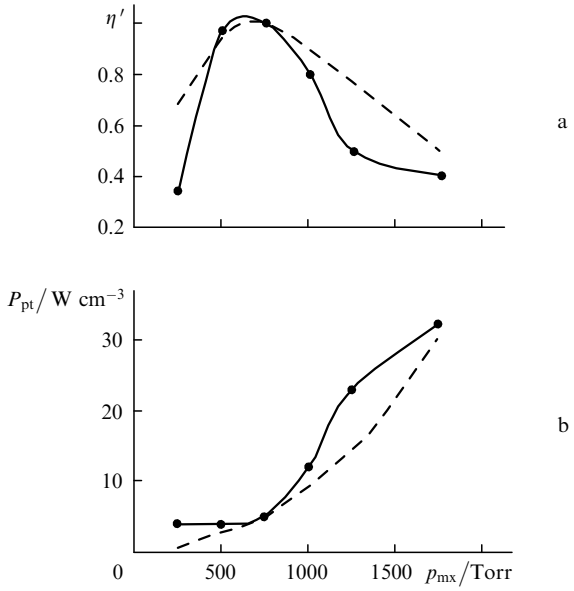

Рис.5. Experimental (solid curves, [27]) and calculated (dashed curves) dependences of the instantaneous laser efficiency η' for an specific input power of 75 W cm^{-3} (a) and the threshold specific input power P_{pt} (b) for $\lambda = 1.79$ μm on the pressure of the He–Ar mixture for $\delta_{Ar} = 3 \times 10^{-3}$ and $T_e \simeq 0.12 - 0.15$ eV.

The calculations were compared with the experiments [4] on nuclear pumping on the VIR-2M reactor at a low specific input power (about 34 W cm^{-3}). Fig. 6 presents the dependences of the laser power at $\lambda = 1.79$ μm and the threshold neutron flux density on p_{Ar} for a He–Ar mixture with a pressure of 2 bar. In [4], the FWHM of the pump pulse was ~ 3 ms. According to Ref. [26], inert gases with impurity content not higher than 5×10^{-3} % are used in such experiments. The calculations carried out for the experimental conditions [4] took this fact into account. The analysis of the dependences calculated for different summary contents of N_2, O_2, H_2, and H_2O impurities δ_{im} in the range from 0 to 5×10^{-3} % showed that the best agreement with the experiment was obtained for $\delta_{im} = 1.5 \times 10^{-3}$ %. Fig. 6 presents the curves calculated for the 'pure' mixture and for the

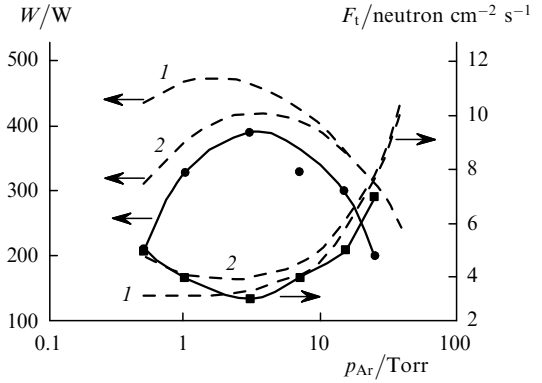

Рис.6. Experimental (solid curves, [4]) and calculated (dashed curves) dependences of the output laser power W and the threshold neutron flux density F_t for $\lambda = 1.79$ μm on the argon pressure in the He–Ar mixture for $p_{mx} = 2$ bar, $T_e \simeq 0.075 - 0.12$ eV, and mixture purity of 100 (*1*) and 99.9985 % (*2*).

mixture with $\delta_{im} = 1.5 \times 10^{-3}$ %. One can see that impurities are of substantial importance for small p_{Ar} and that their effect on laser characteristics at high p_{Ar} is insignificant. The maximum output laser powers W and the minimum threshold neutron flux densities F_t were achieved at $p_{Ar} = 3$ Torr. They were equal to 390 W and 3.2×10^{14} neutron cm^{-2} s^{-1} in the experiment and 420 W and 4×10^{14} neutron cm^{-2} s^{-1} in the calculation.

3.2. Interpretation of the results

The behaviour of the curves in Figs 2–6 can be explained within the framework of our model in the following way. First, the concentration of Ar^+ ions increases from zero and the concentrations of molecular He_2^+ ions and metastable He^* atoms in reactions (11)–(13) decrease with increasing relative argon content in a mixture. The probability of dissociative recombination of He_2^+ ions, which is the dominant channel of electron loss under these conditions, decreases, which causes an increase in their concentration. As a result, the flux of three-body recombination of Ar^+ ions with electrons in reactions (20) and (21), which populates the upper laser level, increases. For $\delta_{Ar} > 10^{-3}$, all the pump energy is transferred from helium components to argon components.

As δ_{Ar} is increased further, the channel of conversion of atomic argon ions into molecular ions in reaction (4) and charge exchange reaction (7) with participation of $HeAr^+$ ions becomes more significant. The concentration of molecular Ar_2^+ ions increases and the contribution of dissociative recombination of these ions (19) to the pumping of the upper laser level also increases. As a result, the flux corresponding to the channel of electron loss during dissociative recombination of Ar_2^+ increases, the electron concentration reaches a maximum (at $\delta_{Ar} \simeq 10^{-3}$), and then decreases with increasing δ_{Ar}. Because the total pump flux to the levels lying above the upper active layer during dissociative recombination exceeds a similar TBR flux, a change of the pumping mechanisms causes an increase in the laser efficiency.

The argon pressure at which the pumping mechanism of the upper laser level changes depends on the pump power (the electron concentration), p_{mx}, and is determined by the competition of two pairs of processes, the loss of Ar^+ in TBR processes (20), (21) and in conversion reaction (4) and the disintegration of $HeAr^+$ ions in reaction (6) and in charge exchange reaction (7) with participation of $HeAr^+$ and Ar. The argon pressure at which the competition of these processes begins is higher for high-power electron-beam pumping, high electron concentration [$N_e = (1-2) \times 10^{14}$ cm^{-3}] and low p_{mx} (Fig. 3b) ($\delta_{Ar} \simeq 10^{-3} - 10^{-2}$), i.e., for weak conversion, and it is lower for weak nuclear pumping (Fig. 6) and a low electron concentration ($N_e < 10^{13}$ cm^{-3}) ($\delta_{Ar} \simeq 3 \cdot 10^{-4} - 10^{-3}$). This also explains a steeper growth of the dependence of the laser efficiency on p_{Ar} (Fig. 4) with increasing p_{mx}, for which the dissociative recombination that pumps the upper laser level with a higher efficiency becomes engaged in the pumping of the upper active layer at a lower p_{Ar}.

In the optimum region of δ_{Ar}, the pumping is provided by dissociative recombination of Ar_2^+ ions. Because of this, the optimum value of δ_{Ar} is determined by the behaviour of the Ar_2^+ ions. The optimum concentration of these ions depends on the ratio of fluxes corresponding to dissociative recombination (19) and conversion of Ar_2^+ into molecular Ar_3^+ ions (8), (9). For a higher electron concentration and lower p_{mx}, conversion becomes competitive with dissociative recombination at a higher p_{Ar}. For instance, in Figs 2 and 3 under electron-beam pumping, the optimum δ_{Ar} is 10^{-2}. When $\delta_{Ar} > 10^{-2}$, an increase in p_{mx} is characterised by a sharper decrease in the output laser energy (Fig. 3) because the flux of the conversion reaction for a fixed electron concentration and a fixed DR flux is proportional to p_{mx}^2.

For a high-power nuclear pumping ($N_e \sim 10^{14}$ cm^{-3}, Fig. 4), the optimum partial argon pressure is lower than for a weak nuclear pumping. It decreases with increasing p_{mx} because conversion increases in importance. Its value at $p_{mx} = 1$, 2, and 3 bar is equal to 5 Torr ($\delta_{Ar} = 6.5 \times 10^{-3}$), 4 Torr ($\delta_{Ar} = 2.5 \times 10^{-3}$), and 3 Torr ($\delta_{Ar} = 1.3 \times 10^{-3}$), respectively. As the specific input power decreases down to 34 W cm^{-3} ($N_e < 10^{13}$ cm^{-3}, Fig. 6), the optimum value of p_{Ar} at $p_{mx} = 2$ bar decreases down to 3 Torr ($\delta_{Ar} = 2 \times 10^{-3}$). For $\delta_{Ar} > 10^{-2}$, laser characteristics become worse because of the quenching of the upper laser level by Ar atoms and a decrease in the cross section for stimulated emission.

The presence of the optimum p_{mx} (Fig. 3a, curves *4–6*) is determined by several factors. For $\delta_{Ar} < 10^{-2}$ (Fig. 3b, curves *4* and *5*), the deterioration of the output radiation parameters with increasing p_{mx} above the optimum value is associated with the quenching of the upper laser level by He atoms and a decrease in the cross section for stimulated emission because of an increase in spectral broadening of the laser line by He atoms. For electron-beam pumping with a higher power (a higher power of output radiation), the difference in the fluxes of induced and other transitions from the upper laser level is stronger than in the case of a weaker nuclear pumping. Because of this, the sensitivity of the dependences of the output laser characteristics as functions of p_{mx} to these two processes becomes stronger with decreasing pump power (Figs 4 and 5). Moreover, in the case of electron-beam pumping, the quenching of the upper laser level by helium is levelled by electron quenching. Because of this, the optimum value of p_{mx} for electron-beam pumping (with a higher electron concentration) is higher (1.5–2 bar) than for nuclear pumping (1 atm, Figs 4 and 5). For $\delta_{Ar} > 10^{-2}$, the conversion of Ar_2^+ into Ar_3^+ (8), (9) becomes competitive with dissociative recombination of Ar_2^+ molecular ions. For a fixed ratio of components (Fig. 3b), the DR flux does nor change with pressure, whereas the conversion flux is proportional to p_{mx}^2. Because of this, the optimum value of p_{mx} shifts to the low-pressure region with increasing δ_{Ar} (Fig. 3b).

4. Optimisation of the nuclear-pumped Ar–Xe laser

For the He–Ar laser pumped by the VIR-2M reactor [2, 26], we performed complete optimisation of energy parameters for lasing at 1.79 μm. The results of optimisation are presented in Fig. 7. It shows the dependences of the laser efficiency η and the total output laser power W on the mixture pressure p_{mx} in the absence of impurities. One can see that the efficiency weakly varies from 1 to 1.18 % in the range $p_{mx} =$ 0.25–1.25 bar. Each point on the curves is a result of optimisation of the specific input power P_p (the maximum neutron flux density for the VIR-2M reactor was assumed to be 2.5×10^{15} neutrons cm^{-2} s^{-1}), the argon pressure p_{Ar}, and the reflectivity of cavity mirrors R. Each point in the given range of pressures belongs to a rather wide domain of variation of these parameters ($p_{Ar} = 0.5 - 5$ Torr, $P_p = 15 - 45$ W cm^{-3}, $R = 0.85\,\% - 0.98\,\%$) in which the laser efficiency

remains almost unchanged. A maximum laser efficiency of 1.18 % is obtained for $p_{mx} = 0.75$ bar, $p_{Ar} = 2$ Torr, $P_p = 30$ W cm^{-3}, and $R = 98$ %.

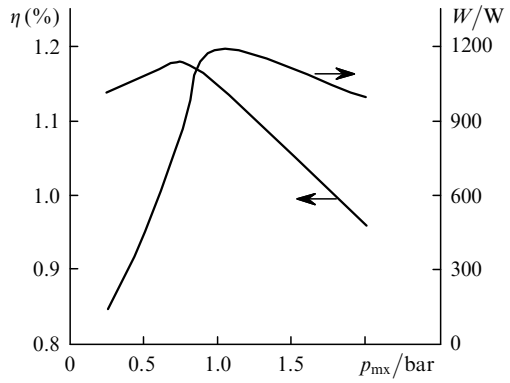

Рис.7. Dependences of the laser efficiency η and the total output laser power W for $\lambda = 1.79$ μm on the pressure of the He – Ar mixture excited by the VIR-2M reactor (nuclear pumping).

5. Conclusions

We developed a detailed nonstationary kinetic model of a laser operating on transitions of the argon atom at 1.79, 1.27, and 2.4 μm in a He – Ar mixture, which takes into account the presence of N_2, O_2, H_2, and H_2O impurities in the active medium. The model was successfully tested using experiment data on electron-beam- and nuclear-pumped lasers. The numerical simulation suggests the following conclusions:

(1) The dominant mechanisms of pumping the upper laser level of IR transitions in the helium atom are the dissociative recombination of molecular Ar_2^+ ions with electrons and the three-body recombination of Ar^+ ions with electrons. The contribution of each of these mechanisms to the pumping of the upper laser level depends on the argon content in a mixture. The three-body recombination governs the pumping for $\delta_{Ar} < 10^{-3}$. When $\delta_{Ar} > 10^{-3}$, the dominant contribution to the pumping is made by dissociative recombination, which provides the pumping of the upper laser level under optimum lasing conditions.

(2) Metastable and resonance argon states $4s$ and $4s'$ determine energy recirculation in chemiionisation reactions and provide up to 50 % of the pump energy flux.

(3) The presence of the optimum argon pressure is caused by the conversion of Ar_2^+, with participation of helium and argon atoms, into a molecular Ar_3^+ ion.

(4) For a nuclear-pumped laser, the maximum calculated efficiency $\eta = 1.18$ % was obtained for $p_{mx} = 0.75$ bar, $p_{Ar} = 2$ Torr, $P_p = 30$ W cm^{-3}, and $R = 98$ %.

The results of complete optimisation of the He – Ar laser pumped by a hard ioniser under different excitation conditions will be published elsewhere.

References

1. Sereda O V, Tarasenko V F, Fedenev A V, Yakovlenko S I *Kvantovaya Elektron.* **20** 535 (1993) [*Quantum Electron.* **23** 459 (1993)]
2. Karelin A V, Sinyavskii A A, Yakovlenko S I *Kvantovaya Elektron.* **24** 387 (1997) [*Quantum Electron.* **27** 375 (1997)]
3. Voinov A M, Dovbysh L E, Kazakevich A T, Krivonosov V N, Mel'nikov S P, Podmoshenskii I V, Sinyavskii A A *Pisima Zh. Tekh. Fiz.* **5** 422 (1979)
4. Voinov A M, Krivonosov V N, Mel'nikov S P, Mochkaev I N, Sinyavskii A A *Kvantovaya Elektron.* **18** 177 (1991) [*Sov. J. Quantum Electron.* **21** 157 (1991)]
5. Magda E P, Grebyonkin K F, Kryzhanovsky V A *Proc. Intern. Conf. LASER'90* (San Diego, USA, 1990), p. 827
6. Zayarnyi D A, Semenova L V, Ustinovskii N N, Kholin I V, Chugunov A Yu *Kvantovaya Elektron.* **25** 493 (1998) [*Quantum Electron.* **28** 478 (1998)]
7. DeYoung R J *Appl. Phys. Lett.* **38** 297 (1981)
8. Derzhiev V I, Zhidkov A G, Sereda O V, Yakovleno S I *Kratk. Soobshch. Fiz. FIAN* No. 4 34 (1989)
9. Ohwa M, Moratz T J, Kushner M J *J. Appl. Phys.* **66** 5131 (1989)
10. Voinov A M, Mel'nikov S P, Sinyavskii A A *Pis'ma Zh. Tekh. Fiz.* **15** (19) 56 (1989)
11. Klopovskii K S, Luk'yanov A V, Rakhimov A T, Suetin N V *Kvantovaya Elektron.* **16** 205 (1989) [*Sov. J. Quantum Electron.* **19** 133 (1989)]
12. Kolokolov N B, Kudryavtsev A A, Nikitin A G, Romanenko V A *Opt. Spektrosk.* **67** 766 (1989)
13. Deese J E, Hassan H A *AIAA J.* **16** 1030 (1978)
14. Lawton W J, Richards J B, Newmam L A *J. Appl. Phys.* **50** 3888 (1979)
15. Witteman W J, Gielkens S W A, Tskhai V N, Peters P J *IEEE J. Quantum Electron.* **34** 250 (1998)
16. Karelin A V, Simakova O V *Kvantovaya Elektron.* **28** 121 (1999) [*Quantum Electron.* **29** 678 (1999)]
17. Karelin A V, Simakova O V *Kvantovaya Elektron.* **28** 129 (1999) [*Quantum Electron.* **29** 687 (1999)]
18. Peters P J M, Mei Q-Ch, Witteman W J *Appl. Phys. B* **47** 187 (1988)
19. Ulrich A, Busch B, Krotz W, Ribitzki G, Weiser J *Proceedings of the Conference on the Physics of Nuclear-Excited Plasma and Problems of Nuclear-Pumped Lasers* (Obninsk, 1993, Vol. 1) p. 54
20. Basov N G, Baranov V V, Danilychev V A, Dudin A Yu, Zayarnyi D A, et al. *Kvantovaya Elektron.* **13** 482 (1986) [*Sov. J. Quantum Electron.* **16** 316 (1986)
21. Basov N G, Baranov V V, Danilychev V A, Dudin A Yu, Zayarnyi D A, et al. *Kvantovaya Elektron.* **13** 488 (1986) [*Sov. J. Quantum Electron.* **16** 320 (1986)
22. Basov N G, Danilychev V A, Kholin I V *Izv. Akad. Nauk SSSR, Ser. Fiz.* **50** 779 (1986)
23. Dudin A Yu, Zayarnyi D A, Semenova D V, Usitnovskii N N, Kholin I V, Chugunov A Yu *Kvantovaya Elektron.* **18** 921 (1991) [*Sov. J. Quantum Electron.* **21** 833 (1991)]
24. Chapovsky P L, Lisitsyn V N, Sorokin A R *Opt. Commun.* **16** 33 (1976)
25. Berkeliev B M, Dolgikh V A, Rudoi I G, Soroka A M *Laser Phys.* **3** 989 (1993)
26. Konak A I, Mel'nikov S P, Porkhaev V V, Sinyavskii A A *Kvantovaya Elektron.* **22** 537 (1995) [*Quantum Electron.* **25** 511 (1995)]
27. Hebner G A, Hays G N *J. Appl. Phys.* **71** 1610 (1992)
28. Hebner G A, Hays G N *IEEE J. Quantum Electron.* **29** 2356 (1993)
29. Bochkov A V, Kryzhanovsky V A, Magda E P *Proc. ICENES'98* (Tel-Aviv, 1998, Vol. 2) p. 868
30. DeYang R J, Jalufka N W, Hohl F *Raketnaya Tekn. Kosmonavt.* **16** 991 (1978)
31. Jalufka N W, DeYoung R J, Hohl F, Williams M D *Appl. Phys. Lett.* **29** 188 (1976)
32. DeYoung R J, Hohl F *IEEE J. Quantum Electron.* **16** 1114 (1980)
33. Mel'nikov S P, Sinyavskii A A *Zh. Tekh. Fiz.* **62** (6) 159 (1992)
34. Shon J W, Kushner M J *J. Appl. Phys.* **75** 1883 (1994)
35. Wilson J W, DeYoung R J, Harries W L *J. Appl. Phys.* **50** 1226 (1979)
36. Ivanov V A *Usp. Fiz. Nauk* **162** (1) 35 (1992)
37. Boichenko A M, Derzhiev V I, Zhidkov A G, Karelin A V, Koval' A V, Protopopov S V, Sereda O V, Ternovskii I M, Terskikh A O, Yurovskii V A, Yakovlenko S I Preprint No. 282 (Moscow: General Physics Institute, Russian Academy of Sciences, 1987)

38. Van Regemorter H *Astrophys. J* **136** 906 (1962)
39. Aymor M, Coulombe M *Atomic Data Nucl. Data Tables* **21** 537 (1978)
40. Lilly R A *J. Opt. Soc. Am.* **66** 245 (1976)
41. Derzhiev V I, Zhidkov A G, Yakovlenko S I *Izluchenie Ionov v Neravnovesnoi Plotnoi Plazme* (Emission of Ions in Nonequilibrium Dense Plasmas) (Moscow: Energoatomizdat, 1986) p. 160
42. Molchanov A G *Trudy Fiz. Inst. Akad. Nauk SSSR* **171** 54 (1986)
43. Boichenko A M, Karelin A V, Yakovlenko S I *Kvantovaya Electron.* **22** 547 (1995) [*Quantum Electron.* **25** 521 (1995)]
44. Karelin A V, Sereda O V, Kharitinov V V, et al. *Atomnaya Energ.* **61** 44 (1986)
45. Azimdzhanov B A, Arslanbekob G U, Bunkin F V, Derzhiev V I, Zhidkov A G, Yurovskii V A, Yakovlenko S I *Kvantovaya Elektron.* **12** 1557 (1985) [*Sov. J. Quantum Electron.* **15** 1029 (1985)]
46. Karelin A V, Yakovlenko S I *Kvantovaya Elektron.* **22** 769 (1995) [*Quantum Electron.* **22** 739 (1995)]
47. Kannari F, Suda A, Obara M, Fujioka T *IEEE J. Quantum Electron.* **19** 1587 (1983)
48. Zhiglinskii (Ed.) *Spravochnik Konstant Elementarnykh Protsessov s Uchastiem Ionov, Electronov, Photonov* (Handbook of Constants of Elementary Processes Involving of Ions, Electrons and Photons (St. Petersburg: St. Petersburg University, 1994)
49. Virin L I, Dzhagashanyan R V, Karachentsev G V, Potapov V K, Tal'roze V L *Ionno-Molekulyarnye Reaktsii v Gazakh* (Ion-Molecular Reactions in Gases) (Moscow: Nauka, 1979) p. 548
50. Smirnov B M *Kompleksnye Iony* (Complex Ions) (Moscow: Nauka, 1983)
51. Biberman L A, Vorob'ev V S, Yakubov V A *Kinetika Neravnovesnoi Nizkotemperaturnoi Plazmy* (Kinetics of a Nonequilibrium Low-Temperature Plasma) (Moscow: Nauka, 1982)
52. Kolokolov N B *Khim. Plazmy* No. 12 56 (1985)
53. Dickinson A S, Roberts R E, Bernstein R B *J. Phys. B* **5** 355 (1972)
54. Nemets O F, Gofman Yu V *Spravochnik po Yadernoi Fizike* (Handbook of Nuclear Physics) (Kiev: Naukova Dumka, 1975)
55. Zayarnyi D A, Semenova L V, Ustinovskii N N, Kholin I V, Chugunov A Yu *Kvantovaya Elektron.* **25** 229 (1998) [*Quantum Electron.* **28** 221 (1998)]
56. Karelin A V, Simakova O V *Kvantovaya Electron.* **25** 319 (1998) [*Quantum Electron.* **28** 307 (1998)]
57. Karelin A V, Simakova O V *Kvantovaya Electron.* **25** 779 (1998) [*Quantum Electron.* **28** 757 (1998)]
58. Kryzhanovskii V A, Magda E P *Trudy Konferentsii po Fizike Yadernogo-Vozbuzhdaemoi Plazmy i Problemam Lazerov s Yadernoi Nakachkoi,* Obninsk, 1992 (Proceedings of the Conference on Nuclear-Excited Plasma and Problems of Nuclear-Pumped Lasers, Obninsk, 1992, Vol. 3) p. 136
59. Magda E P *Trudy Konferentsii po Fizike Yadernogo-Vozbuzhdaemoi Plazmy i Problemam Lazerov s Yadernoi Nakachkoi,* Obninsk, 1992 (Proceedings of the Conference on Nuclear-Excited Plasma and Problems of Nuclear-Pumped Lasers, Obninsk, 1992, Vol. 1) p. 65